ADVANCED MATERIALS
www.advmat.de

Orthogonal Images Concealed Within a Responsive 6-Dimensional Hypersurface

*Yerzhan S. Zholdassov, Daniel J. Valles, Samiha Uddin, Joanna Korpanty, Nathan C. Gianneschi, and Adam B. Braunschweig**

A photochemical printer, equipped with a digital micromirror device (DMD), leads to the rapid elucidation of the kinetics of the surface-initiated atom-transfer radical photopolymerization of *N*,*N*-dimethylacrylamide (DMA) and *N*-isopropylacrylamide (NIPAM) monomers. This effort reveals conditions where polymer brushes of identical heights can be grown from each monomer. With these data, hidden images are created that appear upon heating the substrate above the lower critical solution temperature (LCST) of polyNIPAM. By introducing a third monomer, methacryloxyethyl thiocarbamoyl rhodamine B, a second, orthogonal image appears upon UV-irradiation. With these studies, it is shown how a new photochemical printer accelerates discovery, creates arbitrary patterns, and addresses long-standing problems in brush polymer and surface chemistry. With this technology in hand a new method is demonstrated to encrypt data within hypersurfaces.

1. Introduction

Steganography—the practice of concealing a secret message within a file or image—retains a central role in applications ranging from counterfeit prevention to avoiding surveillance.[1] The first documented example appears in the History of Herodotus,[2] which relates the story of an emissary who had a message tattooed into his head that was revealed upon shaving. Ever since, developing increasingly sophisticated steganographic methods has been a focus of statecraft and spycraft. One emphasis in this field has been on the development of "invisible inks" whose messages appear in response to an external stimulus. As late as World War II, fruit juices, urine, and vinegar—inks that darken upon heating—were still used to transmit messages clandestinely. Modern invisible ink schemes invoke fluorescent chemicals,[3–6] metal-organic frameworks,[7] nanoparticles,[8,9] DNA,[10,11] proteins,[12,13] and even living organisms,[14] but in the cat-and-mouse world of steganography, there will always be a need for new inks that reveal hidden messages in response to an appropriate stimulus.

Here we report new approaches to concealing information that rely upon creating microscale patterns composed of different polymer brushes, where at least one has an optically detectable response to external stimuli. In the first, thermoresponsive poly(*N*-isopropylacrylamide) (pNIPAM) brushes are patterned alongside nonresponsive poly(*N*,*N*-dimethylacrylamide) (pDMA) polymers of the same height (**Figure 1**A). Upon heating in water above their lower critical solution temperature (LCST) of 32 °C,[15–17] the pNIPAM brushes collapse, while the pDMA brushes remain unchanged (Figure 1B), thereby resulting in a change in contrast visible to the naked eye that reveals the hidden message. While such a steganographic system is conceptually simple, achieving it is not and requires addressing several major challenges in brush polymer and surface chemistries. Essentially, this application demands a printing method that can control five independent parameters of each pixel in the polymer brush pattern—the x and y position on the surface, the height of the brushes, their chemical composition, and their changes in time. By our recently coined terminology,[18] such a pattern would be designated a "5D hypersurface." The two major bottlenecks to creating these steganographic 5D hypersurface are: (i) finding conditions to print brushes of different chemical composition with the same heights, and (ii) printing these brushes into arbitrary patterns and with microscale dimensions. The former requires an in-depth understanding of the polymerization kinetics of both

Y. S. Zholdassov, D. J. Valles, S. Uddin, Prof. A. B. Braunschweig
The Advanced Science Research Center at the Graduate Center
of the City University of the New York
85 St. Nicholas Terrace, New York, NY 10031, USA
E-mail: abraunschweig@gc.cuny.edu
Y. S. Zholdassov, D. J. Valles, S. Uddin, Prof. A. B. Braunschweig
Department of Chemistry
Hunter College
695 Park Avenue, New York, NY 10065, USA
Y. S. Zholdassov, D. J. Valles, Prof. A. B. Braunschweig
The Ph.D. Program in Chemistry
Graduate Center of the City University of New York
365 Fifth Avenue, New York, NY 10016, USA
J. Korpanty, Prof. N. C. Gianneschi
Department of Chemistry
Northwestern University
Evanston, IL 60208, USA
Prof. N. C. Gianneschi
Department of Materials Science and Engineering
Northwestern University
Evanston, IL 60208, USA
Prof. N. C. Gianneschi
Department of Biomedical Engineering
Northwestern University
Evanston, IL 60208, USA
The ORCID identification number(s) for the author(s) of this article can be found under https://doi.org/10.1002/adma.202100803.

DOI: 10.1002/adma.202100803

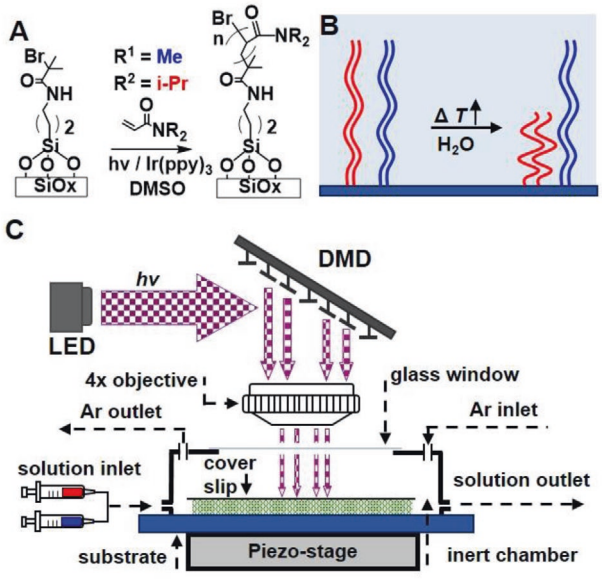

Figure 1. A) Surface-initiated atom-transfer radical photopolymerization (SI-ATRP) to create grafted-from brush polymers with control over height. B) Response of pNIPAM (red) and pDMA (blue) to changes in temperature in H_2O. C) The printer consists of microfluidics to introduce monomer solutions into the reaction chamber, a computer-controlled DMD to direct the light onto the surface, and an inert atmosphere chamber mounted onto a piezoelectric stage.

monomers and may require testing tens or hundreds of different reaction conditions, which remains a major limitation given the serial and low-throughput nature of surface polymerization and characterization techniques.[19–23] The latter necessitates a printer that is compatible with the demanding reaction conditions of advanced polymerization chemistries. Ideally, such a printer could also create features with microscale diameters without using expensive and labor-intensive photomasks so that the printed message can be easily modified to avoid facile cryptanalysis.

2. Results

Recently, we reported a new printing method, termed polymer brush hypersurface photolithography[18] that addresses both the optimization and patterning bottlenecks, and here we apply this tool for the accelerated study of polymer kinetics and the preparation of steganographic hypersurfaces. The printer (Figure 1C) is equipped with a light-emitting diode (LED) that projects light (405 nm) onto a CPU-controlled digital micromirror device (DMD)[24] that possesses ≈750 000 individually addressable mirrors. These mirrors, in turn, reflect the light onto an underlying surface with spatiotemporal control to create patterns via surface-initiated polymer photochemistries,[18,20] resulting in polymer brush pixels with edge-lengths of ≈4 µm. The reactive substrate—in this case a Si/SiO_x surface terminated with an initiator—is placed within a fluid cell encased within an inert atmosphere chamber. Microfluidics deliver different solutions to the fluid cell so that polymer brushes of different composition are printed into arbitrary patterns[25] by coordinating the DMD and the microfluidics.[20,21,26] We previously demonstrated the capabilities of this printer by synthesizing polymer brushes via surface-initiated atom-transfer radical photopolymerization (SI-ATRP).[18] SI-ATRP was chosen because of its broad polymer compatibility[27–31] and because it performs reliably in a variety of different printing platforms.[22,32–37] We showed that the height and composition of the polymer brushes in each pixel could be controlled to create 4D hypersurfaces, and we also prepared block copolymer arrays, where the composition and length of each block could be precisely regulated.[18] What makes these feats possible, and an enabling feature of the printer, is the ability to test tens or hundreds of different reaction conditions in a single print, thereby accelerating the discovery and understanding of the surface-initiated reactions. This acceleration was demonstrated in an investigation of the kinetics of the thiol-(meth)acrylate photopolymerization,[20] where >200 different reaction conditions were tested to show, for the first time, that the thiol-(meth)acrylate reaction shares many of the characteristics of controlled radical polymerizations.

Here we used this printer to find conditions where both pNIPAM and pDMA brushes could be grown to the same height using SI-ATRP. First, reactive substrates were prepared by functionalizing freshly cleaned Si wafers possessing a 500 nm SiO_x layer with aminopropyltriethoxysilane. These amine-terminated wafers were subsequently reacted with α-bromoisobutyryl bromide in CH_2Cl_2 for 24 h to coat the surface with the SI-ATRP initiator. Each step in this process was characterized by X-ray photoelectron spectroscopy (XPS) and contact angle measurements, and the data were consistent with the proposed surface reactions (Figure S3, Supporting Information). The functionalized substrates were moved to a glovebox and placed into the inert atmosphere printing chamber. Reactive solutions composed of monomers (NIPAM or DMA) and tris[2-phenylpyridinato-C^2,N]iridium (III) ($Ir(ppy)_3$) photocatalyst in dimethylsulfoxide (DMSO) were prepared inside the glovebox. For printing, ≈30 µL of the solution was deposited onto the reactive substrate and a cover glass was placed over the solution to prevent light diffraction. For each set of conditions in the kinetic experiments, a pattern of 16 features was projected onto the surface, with each spot representing a different illumination time, t (2–32 min), and each pattern was repeated 192 times across the 4.4 × 3.3 mm printing area to produce statistically significant data (**Figure 2**). The patterned surfaces were washed with EtOH and sonicated in DMSO for 5 min to remove any physisorbed polymer. The heights of the resulting polymer brushes in each feature were then measured by atomic force microscopy (AFM) (Figure 2, inset). Using the sacrificial initiator method,[18,22] the grafting density of the polymers was determined as 0.55 and 0.66 chains nm^{-2} for pNIPAM and pDMA, respectively.

The effects of the major components of the reaction[38]—[monomer], light intensity, and $[Ir(ppy)_3]$—on the growth rate of both pDMA and pNIPAM brushes was investigated (**Figure 3**). First, the DMA and NIPAM concentrations were varied from 1.5 to 9.5 M, while $[Ir(ppy)_3]$ (50 ppm) and light intensity (12.6 mW cm^{-2}) were held constant. At all concentrations, the growth was linear (R^2 = 0.97–0.99) until a plateau in height, h, was reached and growth stopped, which is a growth pattern consistent with previous reports from ourselves[18] and others.[39,40] DMA grew

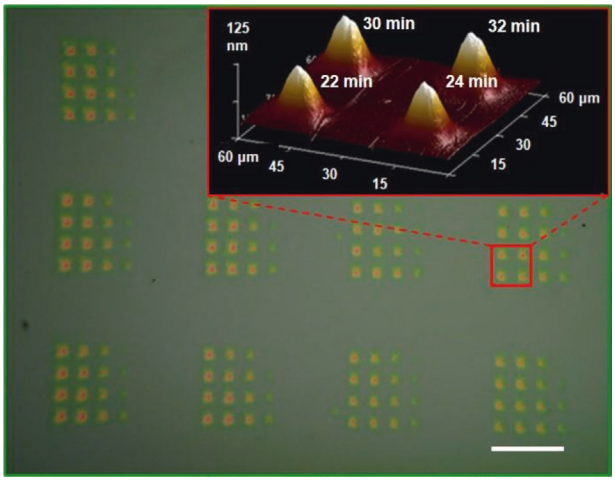

Figure 2. Optical image of pDMA brushes. Printing conditions: [DMA] = 5.5 M; [Ir(ppy)$_3$] = 50 ppm. Light intensity = 12.6 mW cm^{-2}. Inset is 3D AFM images (contact mode) of the pDMA brushes, where each pixel is printed with a different illumination time. Scale bar is 100 µm.

more rapidly than NIPAM across all conditions. At 1.5 M and 20 min, the h of DMA brushes was 50.6 ± 1.8 nm with a growth rate, k, of 2.4 nm min^{-1} (Figure 3A), and NIPAM brushes were 26.8 ± 1.4 nm with k of 1.2 nm min^{-1} (Figure 3B). At 9.5 M and in 16 min, the h of the pNIPAM brushes was 124.2 ± 3.4 nm, with k of 6.6 nm min^{-1}, whereas under the same printing conditions the pDMA brushes expanded laterally and began to grow outside the intended area, which rendered feature height measurements too inaccurate to report (Figure S6E, Supporting Information). Under this concentration range, the change in k with concentration (dk/dC) is 1.1 and 0.7 nm L min^{-1} mol^{-1} for pDMA (R^2 = 0.98) and pNIPAM (R^2 = 0.98), respectively (Figure 3C). The effect of increasing light intensity on the k of both polymers was subsequently investigated. Light intensity was varied from 2.9 to 23.5 mW cm^{-2} at 50 ppm [Ir(ppy)$_3$] and 7.5 M [monomer]. In every pattern, h of polymer brushes increases linearly with t until plateauing, with k ranging from 2.79 to 8.39 nm min^{-1} for DMA (Figure 3D) and 1.23 to 3.67 nm min^{-1} for NIPAM (Figure 3E). For both polymers, k increased linearly with light intensity up to 15.4 mW cm^{-2}, at which point k ceased increasing, which is consistent with previous

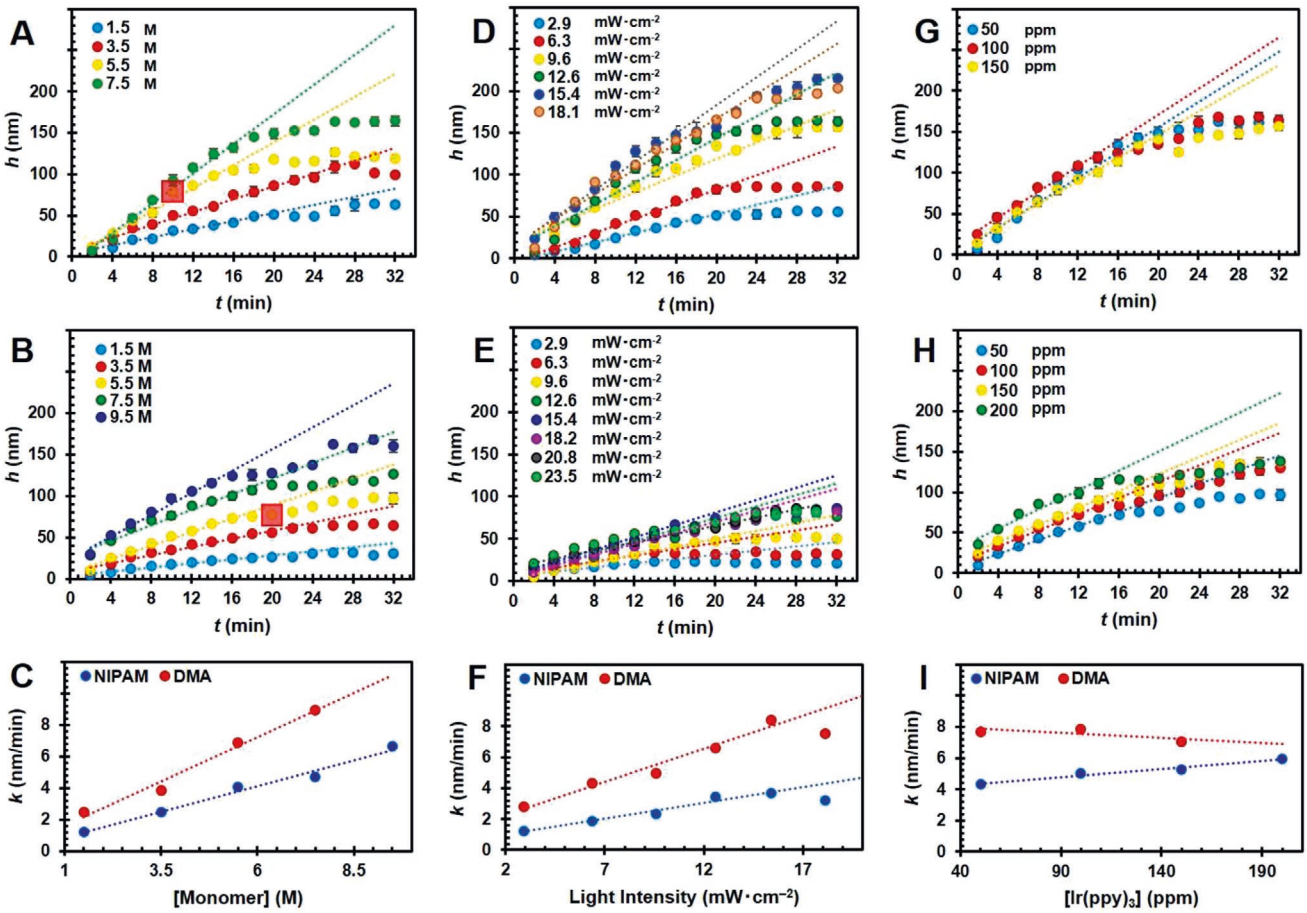

Figure 3. A) Growth of pDMA polymer brushes at varying [DMA] (light intensity = 12.6 mW cm^{-2}; [Ir(ppy)$_3$] = 50 ppm). B) Growth of pNIPAM polymer brushes varying [NIPAM] (light intensity = 12.6 mW cm^{-2}; [Ir(ppy)$_3$] = 50 ppm. C) k vs [Monomer]. D) Growth of pDMA polymer brushes varying light intensity ([DMA]= 7.5 M; [Ir(ppy)$_3$] = 50 ppm). E) The growth of pNIPAM polymer brushes varying light intensity ([NIPAM] = 7.5 M; [Ir(ppy)$_3$] = 50 ppm). F) k vs light intensity G) Growth of pDMA polymer brushes at varying [Ir(ppy)$_3$] (light intensity = 12.6 mW cm^{-2}; [DMA] = 7.5 M). H) The growth of pNIPAM polymer brushes varying [Ir(ppy)$_3$] (light intensity = 12.6 mW cm^{-2}; [NIPAM] = 7.5 M). I) k vs [Ir(ppy)$_3$]. The red boxes in (A) and (B) indicate the conditions used to prepare 5D hypersurfaces where pNIPAM and pDMA are grown to identical heights.

observations.[18,20] The (dk/dI) = 0.43 nm cm^2 min^{-1} mW^{-1} for pDMA (R^2 = 0.97) and 0.21 nm cm^2 min^{-1} mW^{-1} for pNIPAM (R^2 = 0.97) (Figure 3F). Finally, the concentration of the [Ir(ppy)$_3$] was varied from 0 to 200 ppm (Figure 3G,H) at a light intensity of 12.6 mW cm^{-2} and 7.5 M of monomers. While no polymer features were observed in the absence of [Ir(ppy)$_3$], in the tested range of 50–150 ppm, the change in k was minimal and within the errors of the measurement. At longer times (>30 min) at 200 ppm, the features hollow in the middle (Figure S4G,H, Supporting Information), which is consistent with our previous studies.[20] In summary, over 400 different polymerizations conditions were tested, which provided the necessary understanding of the polymerization kinetics, such that printing conditions could be selected to grow pNIPAM and pDMA into brushes of precisely desired h at each pixel within a pattern.

Experiments were performed to quantify the swelling-collapsing transition of the pNIPAM brushes in response to changes in T to ensure that an appreciable change in h would occur so that the T-responsive images could be easily observed optically. Previous studies reported an increase in the change in pNIPAM height, Δh, on the pNIPAM brush number-averaged molecular weight (M_n).[41–43] To quantify this collapse, pNIPAM brushes were printed with varying t (5, 10, 15 min) on the same surface (**Figure 4**A; Figure S12A, Supporting Information), which increases measurement accuracy by reducing batch-to-batch variation. The h of the polymer brushes were measured by AFM in air and in deionized H_2O (Milli-Q 18 MΩ) at 25 and 45 °C, which are below and above the pNIPAM LCST, respectively. The swelling ratio, which is defined as the ratio of hydrated polymer brush thickness to the dry brush thickness at 25 °C, increased with increasing thickness (Figure S11, Supporting Information). This finding is in contrast to Leckband[43] and Bureau,[44] who reported that the swelling ratio and thickness are inversely related. We hypothesize these contradictory results may arise from differences in grafting density between our own and those previously studied. We then determined the collapsing coefficient ($\Delta h/h_0$) in H_2O by measuring pNIPAM and pDMA at 25 and at 45 °C, which are below and above the pNIPAM LCST, respectively (Figure 4A). At 25 °C, the pNIPAM brushes had heights of 80, 140, and 202 nm. Upon heating to 45 °C, these were reduced to 27, 44, and 69 nm, respectively (Figure S12A, Supporting Information). The first finding that we observe that the difference in h between the swollen and the collapsed states was larger (>65%) than the maximum change reported by Plunkett[41] (≈30%) or Wanless[42] (≈46%); however, it is known that h is dependent upon grafting density, and so differences in grafting density may account for these observed differences. The second is that regardless of initial solvated brush height, h_0, at 25 °C in H_2O, the collapsing coefficient was remarkably constant, with a value of 0.67 ± 0.02 (Figure 4A, purple line). As a control, the same experiments were performed on pDMA, whose h remained relatively unchanged: h decreasing slightly for the

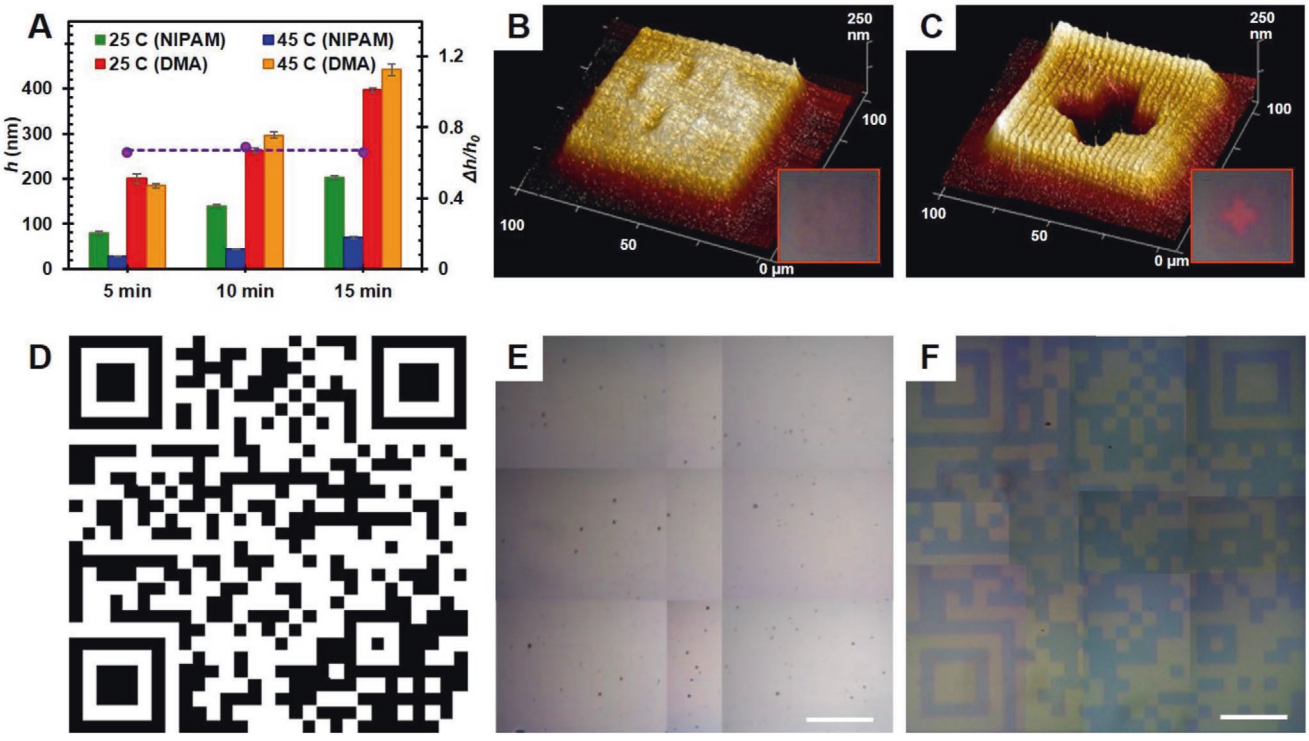

Figure 4. A) pNIPAM polymer brush heights, h, in H_2O at different T. Times are exposure during the growth of the polymers. The green bars are h of pNIPAM at 25 °C, the blue bars are h of pNIPAM at 45 °C, the red bars are h of PDMA at 25 °C, and the orange bars are h of PDMA at 45 °C. The purple dots are the collapsing coefficients ($\Delta h/h_0$) of the pNIPAM brushes, with the dotted line demonstrating that the collapsing coefficient is independent of initial pNIPAM h. B) 3D AFM feature of hidden image in H_2O at 25 °C. C) 3D AFM feature of hidden image in H_2O at 45 °C. The insets are images taken by optical microscopy (10×). D) QR-code that is the model for the hidden image. E,F) Optical images of 5D steganographic surface in H_2O at 25 °C (E) and 45 °C (F). Scale bars are 100 μm.

shortest polymers and increasing slightly for the tallest polymers upon heating (Figure 4A; Figure S12B, Supporting Information).

Using data from the kinetics studies, pNIPAM and pDMA brushes were printed side-by-side and to equal h to prepare a 5D hypersurfaces with an image that reveals itself upon heating >45 °C in H_2O. pNIPAM and pDMA brushes were printed with dry h of 8 ± 1.1 nm. At 25 °C both polymers swelled up to 54 ± 2 nm, but upon heating to 45 °C pNIPAM shrunk to 16.8 ± 0.8, while h of pDMA remained constant (Figure S13, Supporting Information). To test whether an image could be buried within these patterns, we first printed a cross of pNIPAM within a square of DMA (Figure 4B). Upon heating to 45 °C, the pNIPAM collapses, which increases the optical contrast, and the pNIPAM cross becomes darker than its pDMA surroundings (Figure 4C inset). The increasing contrast is related to the increased density of pNIPAM at T above the LCST.[45,46] To show that this steganographic method can be combined with the printer's ability to prepare arbitrary patterns over large areas, we hid a QR code within a pattern composed of pDMA and pNIPAM brushes. Upon heating in H_2O, a hidden image is revealed, and distinct borders between pNIPAM and pDMA brushes are clearly visible by optical microscopy (Figure 4F).

Capitalizing upon the living nature of the SI-ATRP, and the ability to introduce reagents sequentially into the printing chamber with the integrated microfluidics, we created 6D hypersurfaces that revealed different images when heated or when exposed to UV light. A first hidden pattern was prepared by printing 30 nm tall pDMA and pNIPAM brushes. While the chain ends remained living, a solution containing (methacryloxyethyl thiocarbamoyl rhodamine B (RMA) fluorescent monomer mixed with DMA in a 1:1500 ratio[18] was introduced into the fluid cell. A third layer of 10 nm of the fluorescent layer was printed off of the living chain ends that was different than either the pNIPAM or pDMA patterns (**Figure 5**). Under ambient conditions no pattern is seen, whereas upon exposure to UV light a tetrahedral carbon is observed. In the same location, but instead upon heating above the pNIPAM LCST in H_2O, a benzene ring is revealed. Thus a 6D hypersurface

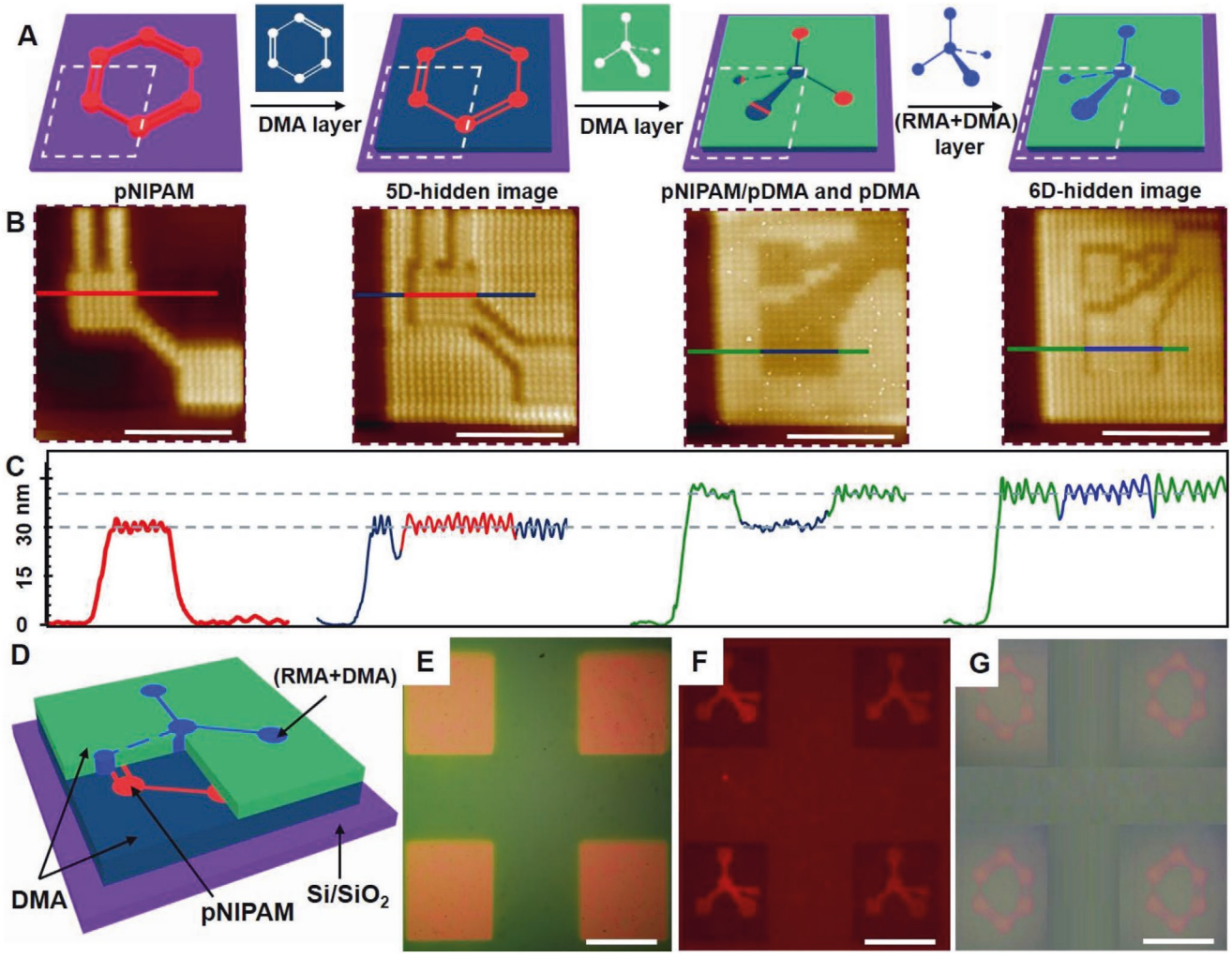

Figure 5. A) The preparation of the 6D hidden image. B) AFM images of features after each step. Scale bar is 50 µm. C) Height of each feature after each step. D) Structure of the 6D hidden image. E) Optical image of the 6D hidden image. Scale bar is 200 µm. F) Revealing the 1st hidden image under UV-light. Fluorescence image of the hidden image (λ_{ex} =530–550 nm, barrier filter λ_{em} =575nm). Scale bar is 200 µm. G) Revealing 2nd hidden image by applying heat in H_2O. Optical image of the hidden image. Scale bar is 200 µm.

has been prepared, where pixels in the pattern are defined by *x,y* position, *h*, chemical composition, response to heat, and response to light. Moreover, we demonstrate a new paradigm in steganography, where multiple hidden images are embedded within the same hypersurface.

3. Conclusion

We have demonstrated a new method to encrypt data within 5D and 6D hypersurfaces using stimuli-responsive polymer brushes embedded within a forest of nonresponsive brushes. In doing so, we tested >400 different grafted-from printing conditions to investigate thoroughly the effects of [monomer], [$Ir(ppy)_3$], and light intensity on the polymerization kinetics of pNIPAM and pDMA, a feat enabled by a new DMD-enabled printing platform. We found that the rates increased linearly with all three, and that the collapsing coefficient of pNIPAM is independent of brush height. Finally, by heating a surface composed of pNIPAM and pDMA brushes of equal heights, a hidden image was revealed. In addition to validating a new steganographic approach, we have further demonstrated the acceleration in discovery that is possible with this DMD-enabled printer, which will have important implications in scientific disciplines where modulating interfacial structure plays a central role. In the future, we intend to expand the scope of chemistries that can be used to create similar patterns, including controlled radical polymerizations with increased O_2 tolerance.

Supporting Information

Supporting Information is available from the Wiley Online Library or from the author.

Acknowledgements

A.B.B. and N.C.G. acknowledge support from the Department of Defense (MURI 15RT0675), the National Science Foundation (DBI-2032176), and the Surface Science Facility of CUNY Advanced Science Research Center.

Conflict of Interest

The authors declare no conflict of interest.

Data Availability Statement

The data that supports the findings of this study are available in the supplementary material of this article.

Keywords

atom-transfer radical photopolymerization, hypersurfaces, photolithography, polymer brushes, stimuli-responsive systems

Received: January 30, 2021
Revised: February 24, 2021
Published online:

[1] D. Kahn, *The Codebreakers: The Comprehensive History of Secret Communication from Ancient Times to the Internet*, Scribner, New York **1996**.
[2] D. Grene, *Herodotus: The History*, University of Chicago Press, Chicago, IL, USA **1988**.
[3] T. Sarkar, K. Selvakumar, L. Motiei, D. Margulies, *Nat. Commun.* **2016**, *7*, 11374.
[4] T. Mutai, H. Satou, K. Araki, *Nat. Mater.* **2005**, *4*, 685.
[5] X. Hou, C. Ke, C. J. Bruns, P. R. McGonigal, R. B. Pettman, J. F. Stoddart, *Nat. Commun.* **2015**, *6*, 6884.
[6] S.-J. Yoon, J. W. Chung, J. Gierschner, K. S. Kim, M.-G. Choi, D. Kim, S. Y. Park, *J. Am. Chem. Soc.* **2010**, *132*, 13675.
[7] C. Zhang, B. Wang, W. Li, S. Huang, L. Kong, Z. Li, L. Li, *Nat. Commun.* **2017**, *8*, 1138.
[8] I. B. Burgess, L. Mishchenko, B. D. Hatton, M. Kolle, M. Lončar, J. Aizenberg, *J. Am. Chem. Soc.* **2011**, *133*, 12430.
[9] G. Liu, L. Chen, J. Liu, M. Qiu, Z. Xie, J. Chang, Y. Zhang, P. Li, D. Y. Lei, Z. Zheng, *Adv. Mater.* **2018**, *30*, 1801772.
[10] J. Liang, M. Castronovo, G. Scoles, *J. Am. Chem. Soc.* **2012**, *134*, 39.
[11] C. T. Clelland, V. Risca, C. Bancroft, *Nature* **1999**, *399*, 533.
[12] K.-W. Kim, V. Bocharova, J. Halámek, M.-K. Oh, E. Katz, *Biotechnol. Bioeng.* **2011**, *108*, 1100.
[13] L. K. McGoldrick, E. A. Weiss, J. Halámek, *ACS Synth. Biol.* **2019**, *8*, 1655.
[14] M. A. Palacios, E. Benito-Peña, M. Manesse, A. D. Mazzeo, C. N. LaFratta, G. M. Whitesides, D. R. Walt, *Proc. Natl. Acad. Sci. USA* **2011**, *108*, 16510.
[15] M. Heskins, J. E. Guillet, *J. Macromol. Sci.: Part A – Chem.* **1968**, *2*, 1441.
[16] L. Cao, T. Man, J. Zhuang, M. Kruk, *J. Mater. Chem.* **2012**, *22*, 6939.
[17] A. Halperin, M. Kröger, F. M. Winnik, *Angew. Chem., Int. Ed.* **2015**, *54*, 15342.
[18] C. Carbonell, D. Valles, A. M. Wong, A. S. Carlini, M. A. Touve, J. Korpanty, N. C. Gianneschi, A. B. Braunschweig, *Nat. Commun.* **2020**, *11*, 1244.
[19] X. Liu, C. Carbonell, A. B. Braunschweig, *RSC Chem. Soc. Rev.* **2016**, *45*, 6289.
[20] A. M. Wong, D. J. Valles, C. Carbonell, C. L. Chambers, A. Y. Rozenfeld, R. W. Aldasooky, A. B. Braunschweig, *ACS Macro Lett.* **2019**, *8*, 1474.
[21] D. J. Valles, Y. Naeem, C. Carbonell, A. M. Wong, D. R. Mootoo, A. B. Braunschweig, *ACS Biomater. Sci. Eng.* **2019**, *5*, 3131.
[22] R. Barbey, L. Lavanant, D. Paripovic, N. Schüwer, C. Sugnaux, S. Tugulu, H.-A. Klok, *Chem. Rev.* **2009**, *109*, 5437.
[23] X. Zhou, X. Liu, Z. Xie, Z. Zheng, *Nanoscale* **2011**, *3*, 4929.
[24] H. Zhao, J. Sha, X. Wang, Y. Jiang, T. Chen, T. Wu, X. Chen, H. Ji, Y. Gao, L. Xie, Y. Ma, *Lab Chip* **2019**, *19*, 2651.
[25] C. W. Pester, B. Narupai, K. M. Mattson, D. P. Bothman, D. Klinger, K. W. Lee, E. H. Discekici, C. J. Hawker, *Adv. Mater.* **2016**, *28*, 9292.
[26] C. Carbonell, D. J. Valles, A. M. Wong, M. W. Tsui, M. Niang, A. B. Braunschweig, *Chem* **2018**, *4*, 857.
[27] J. O. Zoppe, N. C. Ataman, P. Mocny, J. Wang, J. Moraes, H.-A. Klok, *Chem. Rev.* **2017**, *117*, 1105.
[28] M. Fromel, M. Li, C. W. Pester, *Macromol. Rapid Commun.* **2020**, *41*, 2000177.
[29] K. Matyjaszewski, *Macromolecules* **2012**, *45*, 4015.
[30] K. Matyjaszewski, J. Xia, *Chem. Rev.* **2001**, *101*, 2921.
[31] B. Narupai, Z. A. Page, N. J. Treat, A. J. McGrath, C. W. Pester, E. H. Discekici, N. D. Dolinski, G. F. Meyers, J. Read de Alaniz, C. J. Hawker, *Angew. Chem., Int. Ed.* **2018**, *57*, 13433.
[32] B. P. Fors, C. J. Hawker, *Angew. Chem., Int. Ed.* **2012**, *51*, 8850.
[33] J.-S. Wang, K. Matyjaszewski, *Macromolecules* **1995**, *28*, 7901.
[34] Y. Li, J. Zhang, L. Fang, L. Jiang, W. Liu, T. Wang, L. Cui, H. Sun, B. Yang, *J. Mater. Chem.* **2012**, *22*, 25116.

[35] G. Panzarasa, G. Soliveri, K. Sparnacci, S. Ardizzone, *Chem. Commun.* **2015**, *51*, 7313.
[36] S. J. Ahn, M. Kaholek, W.-K. Lee, B. LaMattina, T. H. LaBean, S. Zauscher, *Adv. Mater.* **2004**, *16*, 2141.
[37] L. Fu, Z. Wang, S. Lathwal, A. E. Enciso, A. Simakova, S. R. Das, A. J. Russell, K. Matyjaszewski, *ACS Macro Lett.* **2018**, *7*, 1248.
[38] K. Matyjaszewski, N. V. Tsarevsky, *J. Am. Chem. Soc.* **2014**, *136*, 6513.
[39] J. E. Poelma, B. P. Fors, G. F. Meyers, J. W. Kramer, C. J. Hawker, *Angew. Chem., Int. Ed.* **2013**, *52*, 6844.
[40] M. Li, M. Fromel, D. Ranaweera, S. Rocha, C. Boyer, C. W. Pester, *ACS Macro Lett.* **2019**, *8*, 374.
[41] K. N. Plunkett, X. Zhu, J. S. Moore, D. E. Leckband, *Langmuir* **2006**, *22*, 4259.
[42] B. A. Humphreys, S. W. Prescott, T. J. Murdoch, A. Nelson, E. P. Gilbert, G. B. Webber, E. J. Wanless, *Soft Matter* **2019**, *15*, 55.
[43] C. Xue, N. Yonet-Tanyeri, N. Brouette, M. Sferrazza, P. V. Braun, D. E. Leckband, *Langmuir* **2011**, *27*, 8810.
[44] I. B. Malham, L. Bureau, *Langmuir* **2010**, *26*, 4762.
[45] C. Wu, X. Wang, *Phys. Rev. Lett.* **1998**, *80*, 4092.
[46] V. Aseyev, S. Hietala, A. Laukkanen, M. Nuopponen, O. Confortini, F. E. Du Prez, H. Tenhu, *Polymer* **2005**, *46*, 7118.